Nuclear Instruments and Methods in Physics Research A 769 (2015) 105–111

Contents lists available at ScienceDirect

Nuclear Instruments and Methods in Physics Research A

journal homepage: www.elsevier.com/locate/nima

Proton response of CEPA4: A novel $LaBr_3(Ce)$–$LaCl_3(Ce)$ phoswich array for high-energy gamma and proton spectroscopy

E. Nácher [a,*], M. Mårtensson [b], O. Tengblad [a], H. Álvarez-Pol [c], M. Bendel [d], D. Cortina-Gil [c], R. Gernhäuser [d], T. Le Bleis [d], A. Maj [e], T. Nilsson [b], A. Perea [a], B. Pietras [c], G. Ribeiro [a], J. Sánchez del Río [a], J. Sánchez Rosado [a], A. Heinz [b], B. Szpak [e], M. Winkel [d], M. Zieblinski [e]

[a] Instituto de Estructura de la Materia, CSIC, E-28006 Madrid, Spain
[b] Chalmers University of Technology, S-41296 Göteborg, Sweden
[c] Universidad de Santiago de Compostela, E-15782, Spain
[d] Technische Universität München, 80333, Germany
[e] Polish Acad. Sci., H Niewodniczanski Inst Nucl Phys, PL-31342 Krakow, Poland

ARTICLE INFO

Article history:
Received 4 August 2014
Received in revised form
16 September 2014
Accepted 25 September 2014
Available online 6 October 2014

Keywords:
Phoswich
$LaBr_3(Ce)$
$LaCl_3(Ce)$
Pulse-shape analysis
Spectroscopy
Proton detector

ABSTRACT

A new phoswich array, for the detection of high-energy protons and gamma rays from nuclear reactions, has been built. This new detector consists of four individual closely packed scintillator detectors, each of them made of 4 cm of $LaBr_3(Ce)$ and 6 cm of $LaCl_3(Ce)$ in phoswich configuration (optically coupled and with a common readout). In this paper we report on the results of a beam test performed at the Bronowice Cyclotron Centre (CCB) in Krakow, showing the response of this versatile instrument to high energy protons (70–230 MeV). Furthermore, for the first time we prove that we can reconstruct the original energy of fast protons ($E > 200$ MeV) which pass through the total length of the crystal while still retaining a good energy resolution.

1. Introduction

1.1. Motivation

Quasifree nucleon-knockout reactions, $(p,2p)$ and (p,pn), by medium and high-energy proton beams, have long been used to study the single-particle properties of bound nucleons inside the nucleus. Reactions at several hundred MeV have sufficient energy to excite deep-hole states maximizing localized interactions and therefore acting as a probe for single-particle properties. Moreover, since the nucleon–nucleon cross-sections are small at these energies, one can approximate that only the knocked-out nucleon participates in the reaction while the influence of the other "spectator" nucleons on the reaction process can be neglected. This is why, in these cases, the knock-out process itself can be treated in the impulse approximation, i.e. as quasifree scattering (QFS). These QFS reactions provided an early test of the reality of deeply bound nuclear shell structures. For a general review on QFS see Refs. [1,2] and for more recent results see Ref. [3].

The $(p,2p)$ reaction experiments are based on the detection of the two outgoing protons in coincidence with an angle of 90° between them in the laboratory system (less than 90° in inverse kinematics experiments). The angular and energy distributions of the outgoing protons, in combination with those of the gamma rays from the de-excitation of the recoil nucleus, reveal the structure (energy and angular momentum) of the hole-states left by the knocked-out proton as long as the detection system is sufficiently good. Within this context, a major challenge in nuclear instrumentation is the design and construction of detectors to determine the complete kinematics of QFS reactions with radioactive beams at relativistic energies. The latter is the goal of the R^3B setup [4] at the future FAIR facility [5,6].

The R^3B Collaboration has proposed and designed an experimental set-up to perform measurements, in complete kinematics, of reactions with radioactive beams at relativistic energies. These beams will be produced and selected using the in-flight production method at the Super-FRS device of the future FAIR facility. One of the sub-detector systems in the R^3B setup will be a gamma-ray and proton calorimeter surrounding the reaction target position. This device is called CALIFA [7] and the Technical Design Report of its Barrel section has already been approved by the FAIR management board [8]. The goal of CALIFA is the simultaneous detection

* Corresponding author.
E-mail address: enrique.nacher@csic.es (E. Nácher).

http://dx.doi.org/10.1016/j.nima.2014.09.067
0168-9002/

of gamma rays and protons. The most forward part of CALIFA, its forward endcap, is called here CEPA, which stands for CALIFA Endcap Phoswich Array. This is the part of the calorimeter which will detect the most energetic gamma rays and protons emerging from the reactions at relativistic energies. As an example, in a typical $(p,2p)$ reaction in inverse kinematics using a beam of ^{12}C at 400 A MeV, around 80% of the outgoing protons within the angular coverage of CEPA will have energies ranging from 200 to 400 MeV. Furthermore, CEPA must be ready to measure not only medium to high-energy protons, but gamma rays of up to 30 MeV as well.

1.2. Detector description

The simultaneous detection of high-energy gamma rays and protons with a reasonably good energy resolution is far from trivial. One possible solution, based on a phoswich configuration, was already presented in Ref. [9]. In that work we tested, for the first time, a small stack of two scintillators optically coupled, for the detection of gamma rays and protons, and demonstrated that, using pulse-shape analysis techniques, one can separate the energy deposited in both scintillator crystals. This small cylinder was the first prototype along the way to the final design of CEPA. Encouraged by our results and the Monte Carlo simulations presented in Ref. [9], we designed a second prototype, namely CEPA4: a composite detector made of four square-shaped phoswich units longer than the cylinder used in Ref. [9]. The goal of such an array is to test, among other things, the canning of four phoswich units in one single aluminum case with just teflon between them, the quality of the optical insulation of the scintillator crystals as well as the exit quartz windows and, finally, the gain in peak efficiency, for the higher proton energies, by applying an energy add-back procedure of the four units. The detector was manufactured by Saint-Gobain [10] and has been recently tested using standard low-energy gamma sources in our local lab, and using high-energy proton beams at the CCB facility in Krakow [11]. In order to distinguish the protons from the gamma rays and, at the same time, obtain information on the entrance point of the proton in the detector, a double-sided Silicon strip detector (DSSSD) has been incorporated in CEPA4. A detailed view of this design is shown in Fig. 1. The design of this prototype, far from the final design of the endcap CEPA, allows for measurements of beta-delayed protons and gamma rays in which the DSSSD is in vacuum, close to the implantation point, and the scintillator part is in air. It should be noted here that, due to technical issues, the signal from the DSSSD was not used in the digital acquisition system during the experiment at CCB as will be detailed later.

Each of the four phoswich units in CEPA4 is comprised of 4 cm of $LaBr_3(Ce)$ and 6 cm of $LaCl_3(Ce)$ optically coupled and with a common readout, namely a photomultiplier tube of type Hamamatsu R5380 (8 stages) with a tapered voltage divider Hamamatsu socket E678-14C designed for this photomultiplier [12]. The maximum supply voltage accepted by this mounting is +1800 V, but the working voltage we have used is +900 V in order to fit the dynamic range and not saturate the output pulses. The cross-section of each crystal is a square of 27 mm of side, and the total length or lateral side of each phoswich unit is 100 mm long (40 mm of $LaBr_3(Ce)$+ 60 mm of $LaCl_3(Ce)$). The four phoswich units are optically insulated from each other by $\approx$ 1 mm of teflon reflector, and they are packed together in an aluminum case 0.5 mm thick. During the tests performed in our local lab we measured energy resolutions of 3.9% at 662 keV for the four $LaBr_3(Ce)$ crystals and 6.5%–7.0% for the $LaCl_3(Ce)$ ones. The DSSSD in front of the entrance window of CEPA4 is made of 16 horizontal strips and 16 vertical strips, each 1 mm wide, covering an active area of 5 $\times$ 5 cm^2. The Si substrate is 0.5 mm thick, which makes it ideal to detect the entrance point of the proton, but not to perform any spectroscopy.

We base the data analysis on the fact that the two scintillators of our phoswich, namely $LaBr_3(Ce)$ and $LaCl_3(Ce)$, have different scintillation properties. In particular, their decay constants are 16 and 28 ns, respectively. This allows us to perform pulse-shape analysis based on integrating the signals in different time regions as described in Ref. [9]. However, this also implies the necessity of using an appropriate signal digitizer to allow for off-line analysis of the electronic signals. For this purpose we chose the VME module CAEN V1742. This device is able to store the shape of the signal at a sampling rate of up to 5 GS/s with a bandwidth $>$ 500 MHz. For further information refer to [13].

2. Beam test at CCB (Krakow)

2.1. Experimental setup

In order to test the response of our prototype CEPA4 to medium and high-energy protons, we used the beams provided by the proton cyclotron at the Bronowice Cyclotron Centre (CCB) in Krakow. This center is a part of the Henryk Niewodniczański Institute of Nuclear Physics Polish Academy of Sciences in Krakow (IFJ PAN) and it is devoted to investigate the application of cyclotrons in scientific research and tumor radiotherapy. The cyclotron at CCB was installed recently and this was the first physics experiment in the hall.

For our measurements we were provided with mono-energetic proton beams at energies ranging from 70 to 235 MeV, with an energy resolution of $\approx$ 0.7% (FWHM). Since the beam current was too

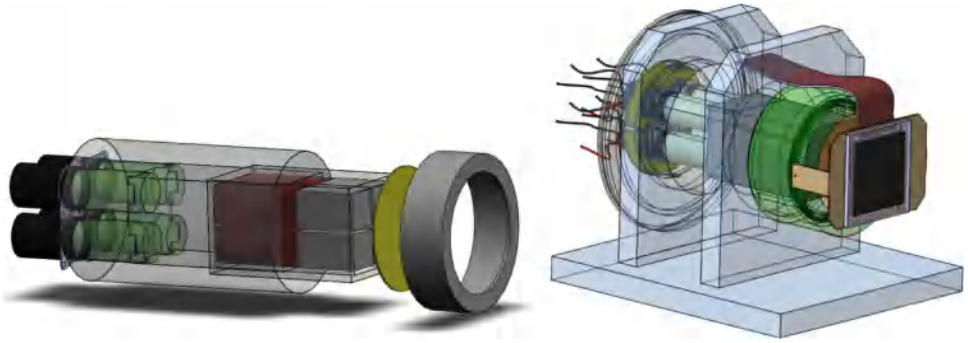

Fig. 1. Detailed scheme of the CEPA4 detector. Left panel: In green there are the four photomultiplier tubes, in red/gray one can see the squared prisms representing the phoswich units, in yellow a thin Al window that keeps the vacuum at the right side of the detector while having the scintillators and photomultipliers in air at the left side. Right panel: Support for CEPA4 and DSSSD coupled to the entrance face, as was mounted for the beam test described in the text. This design allows for a special mounting in which the DSSSD is in vacuum, coupled to a reaction/implantation chamber, while the rest of the device is measuring in air. (For interpretation of the references to color in this figure legend, the reader is referred to the web version of this paper.)

high (≈ 1 nA) to place the detectors directly in front of the beam, we measured the protons originating from the elastic scattering of the original beam on a 50 μm (23 mg/cm^2) thick titanium foil. The measurement was performed in air and with the detector CEPA4 at an angle of 18 degrees with respect to the beam direction. The energy loss due to the scattering angle has been calculated as well as the losses in the target foil at the end of the beam pipe, the DSSSD and the detector casing and, in the worst case (at 70 MeV) amount to less than 2 MeV (0.10 MeV in the Ti foil, 0.89 MeV in the DSSSD, 0.99 MeV in the Al+Teflon) [14]. These calculations have been corroborated by Monte Carlo simulations using the Geant4 code [15] to account for the different possible paths of the protons when entering the detector volume. A schematic view of the setup is shown in Fig. 2.

As far as the data acquisition is concerned, we used two different electronic branches. In the first one, we digitized and stored the electronic signals coming from the anodes of the four photomultiplier tubes, using the VME digitizer CAEN V1742. In order to avoid perturbations in the original shape of the signal, we did not use any pre-amplifier or shaper whatsoever. In the second branch, we used an analog electronic chain and the acquisition system was based on the VME peak-sensing ADC CAEN V785 (see Ref. [13]). For this purpose the signals from both, the photomultiplier tubes and the DSSSD, were treated with the appropriate preamplifier and amplifier/shaper modules from MESYTEC GmbH & Co [16].

2.2. Detector response to medium and high-energy protons

With the setup described above, we measured several different energies of protons to characterize our detector. It is important to understand that, due to the fact that the protons have to pass two different scintillator materials, we cannot have one unique calibration curve that covers the full energy range. On the contrary, we will always refer to three different regions in our spectra: the first region corresponds to proton energies up to 130 MeV, for which the full energy is absorbed in the first crystal ($LaBr_3$). The second region covers the energies above 130 MeV up to the total punch-through energy at around 200 MeV. In this energy range the protons are stopped in the second crystal ($LaCl_3$). The third region, beyond 200 MeV, contains the protons which punch through both crystals and continue traveling beyond. The goal of this work is to distinguish these three regions in our spectra, being able to reconstruct the original energy, even in the cases in which the protons are not stopped in our detector ($E > 200$ MeV).

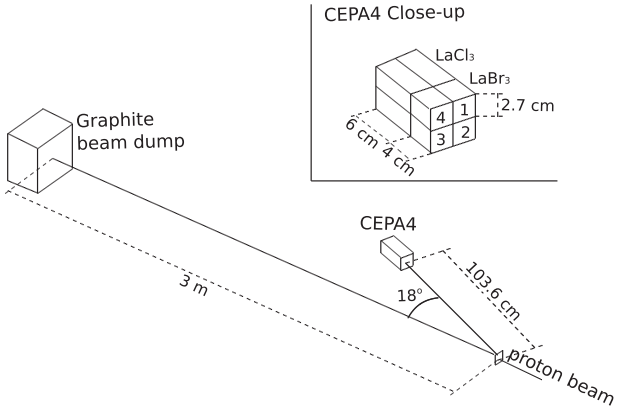

Fig. 2. Experimental setup at CCB (Krakow). The insert shows the geometry and orientation of the four phoswich crystals.

Our first task was to check the linearity of the system (crystal-photomultiplier-digitizer) within the first energy region. One of our concerns was the possible saturation of the photomultiplier tube for a high light yield of the scintillator crystals. With our phoswich configuration this might only happen for energies below 130 MeV since the highest light output occurs when the Bragg peak is entirely within the first crystal. Once the proton energy is enough to produce the Bragg peak in the second crystal the light output is lower as the light yield of $LaBr_3$(Ce) is 1.3 times higher than that of $LaCl_3$(Ce). The left panel of Fig. 3 shows the digitized anode signals as recorded in the CAEN V1742 digitizer for different proton energies in the range 70–120 MeV. A linear regression of the amplitude of these signals as a function of the energy deposited in the crystal produces a correlation coefficient $r=0.997$ and a coefficient of determination $r^2 = 0.994$. This ensures the good linearity of the system and the absence of saturation in the output pulses. Furthermore, the right panel of the same figure shows these signals normalized to their amplitude. The perfect match of the whole pulse shapes guarantees the validity of the pulse-shape analysis independently on the proton energy.

Once the linearity of the system has been checked and confirmed, in order to separate the three energy regions mentioned above and to reconstruct the original energy of the protons, we need to determine the energy deposited in the first and second crystal separately. For this purpose we followed Ref. [9] and analyzed the pulse-shape calculating the integral of the electronic signal (total charge collected by the anode) in three different time intervals, which we call I_{nose}, I_{tail} and I_{total}. These intervals, along with their limits, are shown in Fig. 4.

As explained in the figure, x_0 is the time when the signal passes the threshold and x_p is the time corresponding to the peak, the maximum value of the signal. These two are clear definitions and easy to implement in our algorithm. However, the definitions of x_1 and x_2 are not so clear and require optimization. Data from a

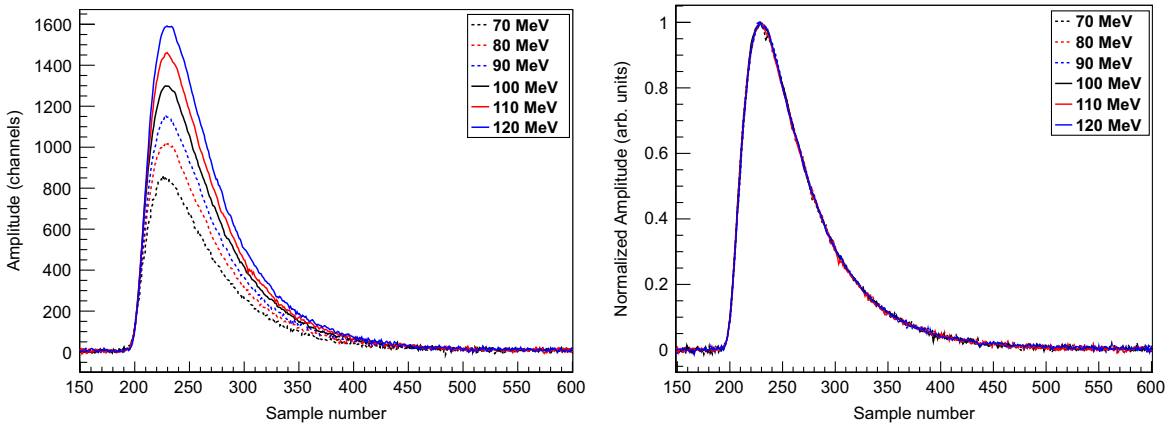

Fig. 3. Left panel: Proton traces recorded by the CAEN V1742 digitizer in the energy range 70–120 MeV. Right panel: The same traces but normalized to their amplitude.

150 MeV run has been chosen as a basis for this purpose. To start with, we have plotted I_{tail} versus I_{total}, which is the first step to separate the energies deposited in both crystals (see Ref. [9]). The resulting 2D plot is shown in Fig. 5. In this plot we can distinguish three main features: the straight line with the smaller slope corresponds to those events that have deposited energy only in the first crystal, namely the $LaBr_3$ scintillator. The straight line with the larger slope corresponds to those events that have deposited energy only in the second crystal, namely the $LaCl_3$ scintillator. Finally, the main spot in between the lines, upper-right corner, corresponds to events in which the 150 MeV protons have been fully absorbed in the phoswich, therefore having deposited energy in both crystals. One might think that, for a monoenergetic beam of protons, all the events should be recorded in this spot and not in the two lines mentioned earlier. However, at these energies the probability of producing nuclear reactions in the $LaBr_3$(Ce) is not negligible and a certain fraction of the incoming protons interacts with the crystal nuclei via knock-out reactions, in which one or several neutrons can be produced. These neutrons normally escape the detector without depositing any energy and therefore these events fall in the line labeled "$LaBr_3$" in Fig. 5 (see Ref. [9] for a deeper study of this type of events using Monte Carlo simulations). On the other hand, the events falling in the line labeled "$LaCl_3$" are due to protons entering directly the second crystal of the phoswich without passing through the first one, mainly coming from scattering in the walls or in the other detectors present in the hall.

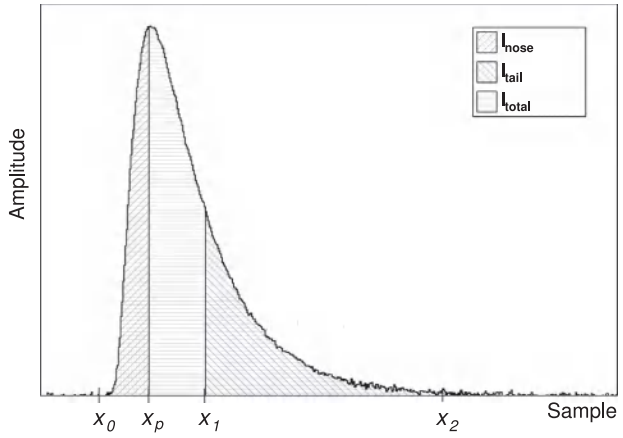

Fig. 4. Electronic signal corresponding to protons at 150 MeV. The integral limits for the pulse-shape analysis are shown: x_0 is the time when the signal goes beyond the threshold, x_p is the time corresponding to the peak, the maximum value of the signal, x_1 is the lower limit of the tail and x_2 is its upper limit (see the text).

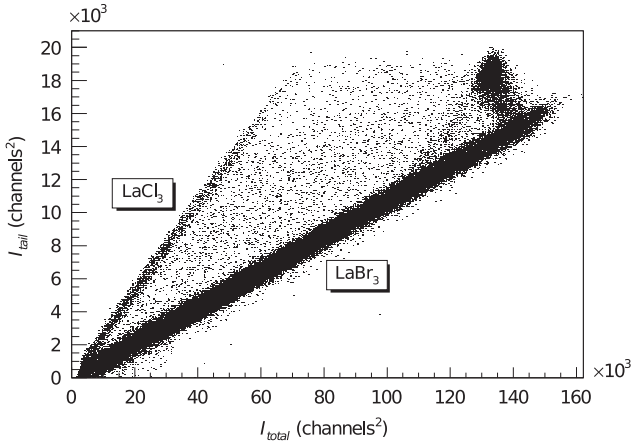

Fig. 5. Two-dimensional I_{tail} *vs* I_{total} plot for 150 MeV protons. The spot between the two lines corresponds to the protons fully absorbed in the detector, whereas the straight lines contain those events leaving only part of their energy in either the first crystal (smaller slope) or the second crystal (larger slope).

For the optimization of the parameters x_1 and x_2 we have used only the events in the full-absorption spot as these are the ones which define the energy resolution of the detector. To do so we have projected the two-dimensional plot of Fig. 5 onto the y-axis and then we have calculated the σ of the resulting Gaussian peak. Minimizing σ_{tail}/I_{tail} as a function of the free parameters x_1 and x_2, we have found an optimal set of values x_1 and x_2 which provides us with the best energy resolution for 150 MeV protons. It turns out that, choosing $x_1 = 100$ samples (20 ns) right to the peak position and $x_2 = 300$ samples (60 ns) right to the peak position, is the combination that produces the best energy resolution (with the CAEN V1745 running at 5 GS/s and 1024 channels per sample).

Once we have determined the appropriate limits for the integrals to analyze the shape of the signal event by event, we can proceed to determine the energy deposited in each crystal by disentangling the scintillation light produced in the $LaBr_3$ crystal from that produced in the $LaCl_3$ one. Looking at Fig. 5 one can deduce that, for each individual crystal, the tail integral is a constant fraction of the total integral:

$$\begin{cases} I_{Br}^{tail} = a_{Br} \cdot I_{Br}^{total} \\ I_{Cl}^{tail} = a_{Cl} \cdot I_{Cl}^{total}, \end{cases} \tag{1}$$

where the subscripts *Br* and *Cl* stand for $LaBr_3$(Ce) and $LaCl_3$(Ce), respectively. Furthermore, the fact that both crystals in the phoswich have a linear response with the energy (guaranteed by the manufacturer and supported by our experimental data shown in Fig. 3), ensures that the integral of the signal (*total* or *tail*) is just the addition of the individual contributions of the two scintillator crystals,

$$\begin{cases} I^{total} = I_{Br}^{total} + I_{Cl}^{total} \\ I^{tail} = I_{Br}^{tail} + I_{Cl}^{tail}. \end{cases} \tag{2}$$

Now, following [9], we can combine these four equations to obtain the separated pulse integrals:

$$\begin{cases} I_{Br}^{total} = \dfrac{I^{tail} - a_{Cl} \cdot I^{total}}{a_{Br} - a_{Cl}} \\ I_{Cl}^{total} = \dfrac{a_{Br} \cdot I^{total} - I^{tail}}{a_{Br} - a_{Cl}}. \end{cases} \tag{3}$$

The constants in these two equations, namely a_{Br} and a_{Cl}, can be obtained by performing linear fits to the two straight lines which appear in Fig. 5 (for different proton energies). These linear fits depend on the crystal, but, to three significant digits they are equal for all the four crystals in CEPA4: $a_{Br} = 0.106$ and $a_{Cl} = 0.260$. At this stage, in order to calibrate our four units and transform these integrals into energy deposited in each piece of the phoswich, we can use the separated pulse integrals of Eq. (3) for different proton energies. We have used proton energies ranging from 70 to 200 MeV, and we have calculated their energy deposition in the two pieces of the phoswich as well as in the other layers that they pass through (Ti foil at the end of the beam pipe, Si at the DSSSD, Al and Teflon at the entrance of CEPA4) by means of a highly detailed Monte Carlo simulation using the Geant4 simulation code [15]. This allows us to obtain the calibration curves for two pieces of scintillator crystals:

$$\begin{cases} \Delta E_{Br} = b_0 + b_1 I_{Br}^{total} \\ \Delta E_{Cl} = b_2 + b_3 I_{Cl}^{total}, \end{cases} \tag{4}$$

and from this point we can measure medium and high-energy protons and separate the energy deposited in the two different crystals for each phoswich unit. An example of such a measurement is shown in Fig. 6. It represents a two-dimensional plot of type ΔE *vs* E, typical of a telescope configuration. This type of plot has been traditionally used for particle identification, and we can actually use it for this purpose as well. However, in our case, the aim of such a representation is to reconstruct the energy of the incident protons even if they have passed through the total length of the phoswich unit. Fig. 6 displays the energy deposited in the $LaBr_3$ versus the total energy deposited in the phoswich unit. An add-back procedure has been used on an event-by-event basis so that we have added the energy deposited in all four crystals. However, we have carried out a multiplicity analysis (number of phoswich units fired per event) and have concluded that very few events do actually deposit energy in more than one phoswich unit, which happens only for the higher energies. In particular, for 90 MeV protons only 1.7% of the events have multiplicity higher than 1, for 150 MeV: 4.5%, and for 220 MeV: 21.2% (of which less than 1% have multiplicity 3).

In the plot we can clearly see the spot corresponding to 90 MeV protons, fully absorbed in the first crystal of the phoswich, namely the $LaBr_3$. Continuing along the diagonal we find the spot of the 130 MeV protons. These are at the limit of absorption in the first crystal, all energies above will pass through the $LaBr_3$ and enter the $LaCl_3$ crystal. One of such examples are the 150 MeV protons that we can see as a spot in the banana corresponding to all the protons stopped in the second crystal. Finally, it is more difficult to visualize, but we have also included the spot which corresponds to the 220 MeV protons that pass through the entire length of the phoswich unit. We can zoom in Fig. 6 pointing at the 220 MeV spot and change to the three-dimensional representation of Fig. 7. In this way we can have an impression of the ability of the CEPA4 detector combined with the pulse-shape analysis to separate the 220 MeV protons that have passed through the detector from the continuum at lower energies. This implies that, with the appropriate unfolding algorithm, one can reconstruct the original energy of the protons even at the energies that push the Bragg peak out of the volume of the detector. Furthermore, at 220 MeV we still separate the peak from the neighboring energies with a resolution of around 7%, but it gets worse as we increase the energy (see next section).

2.3. Energy calibration and resolution

The calibration function which converts the experimental channels (height of the electronic signal) into energy is difficult to define when making use of two-dimensional histograms to separate the different proton energies above 130 MeV. The first stage in our calibration is to perform the appropriate projection in order to transform the two-dimensional histogram into a one-dimensional histogram that can be calibrated. Neither the x-axis, nor the y-axis are proper line for a projection, since none of them reproduces the direction in which the full absorption spot moves when increasing the energy. Looking at Fig. 8 one can clearly see that we need to divide our histogram in three different regions depending on the energy of the incoming protons, and project the points onto three different lines. For energies below 130 MeV we have projected the points onto the line at 45 degrees, namely line A of the figure, as this is the line along which the spots move as the energy increases. For energies above 130 MeV, in which the protons pass through the first crystal and are stopped in the second crystal of the phoswich unit, we have projected onto B, since the full absorption spots move along this line with increasing energies. Finally, after the total punch-through at 200 MeV, the spots move backwards as the energy deposited in both crystals decreases with energy. For this reason we have projected onto the line marked C.

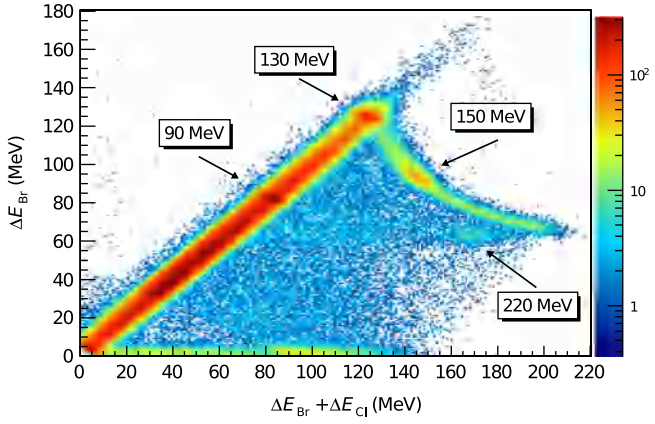

Fig. 6. Two-dimensional $\Delta E-E$ plot for different runs with different proton energies: 90, 130, 150 and 220 MeV. The vertical axis represents the energy deposited in the $LaBr_3$ crystal and the horizontal axis the total energy deposited in the phoswich.

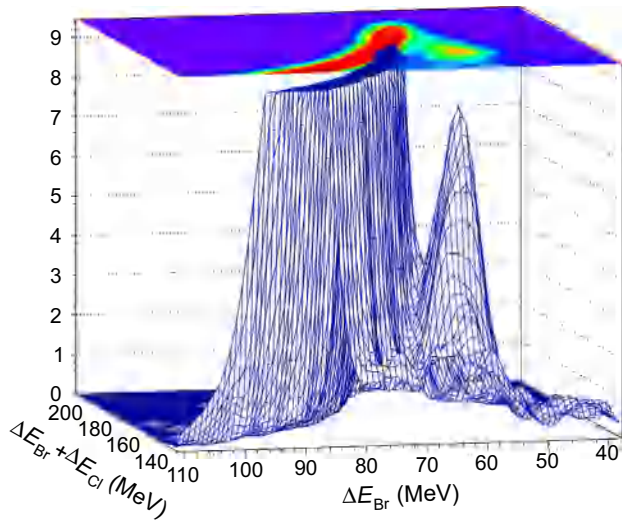

Fig. 7. Same as Fig. 6 in a three-dimensional representation. The graph is zoomed around the spot at 220 MeV and a smoothing has been applied on the data.

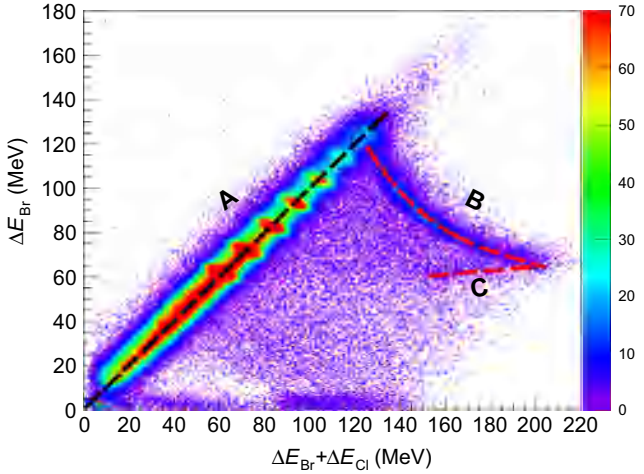

Fig. 8. Two-dimensional $\Delta E-E$ plot for the runs included in the resolution analysis (protons of 70–230 MeV). The 2D histogram has been later projected onto the three lines: A, B and C for the determination of the energy resolution (see the text).

With the histograms projected onto these three lines we have calibrated in energy the new lines, which act as new x-axes, and we have fitted the peaks to Gaussian distributions and calculated the energy resolution as a function of the beam energy. One example of such a projection in region C, after the total punch-through, containing data and fits from two different runs (225 and 235 MeV), is shown in Fig. 9. As we can see we cannot resolve the two peaks as their separation in energy is less than 5%, which is beyond our resolution capabilities in this region.

Analyzing these projections for a whole set of energies from 70 to 235 MeV one can study the energy resolution of the CEPA4 device as a function of the proton energy. In this context we have used the classical definition of energy resolution: $\Delta E/E$, being ΔE the full width at half maximum of the Gaussian fit to the full absorption peak and E the centroid of the peak. This is represented in Fig. 10. Again one can clearly distinguish between the three different regions depending on the position of the Bragg peak in the detector. For energies below 130 MeV (A in Figs. 8 and 10) the energy resolution improves with the proton energy and reaches as low as 3% for 130 MeV protons when analyzing the pulse shapes with the digitizer module. In the figure we have compared the results using the add-back of the four phoswich units (black squares) with those using only one detector (red circles). Furthermore, for this low energy region we have also included the resolution obtained with the analog electronic chain (blue triangles). As the latter includes preamplifier and amplifier/shaper modules, the energy resolution is consistently 1% better than that obtained with the digitizer for the energy range 70–130 MeV, reaching as low as 2% at 130 MeV. Beyond this energy we can only reconstruct the original energy of the protons using the digitizer and the pulse-shape analysis described before. In the intermediate region, which includes energies ranging from 130 to 200 MeV, the resolution starts at 8% for the worst case: 145 MeV, right after the first punch-through. At this energy the protons can pass the boundary between the two crystals for the first time. Then the energy resolution improves with increasing energy again until it reaches 5%, right before the second punch-through (200 MeV). Finally, in the last energy region, namely above 200 MeV (C in the figures), the spots corresponding to 225 and 235 MeV spread a bit more along the line marked as C in Fig. 8. One can still analyze these peaks (see Fig. 8) and obtain the last two points shown in the resolution curve in Fig. 10. In this final high-energy region the energy resolution becomes worse with increasing energy as it is shown in the figure and confirmed with Monte Carlo simulations (see Ref. [9]). However, we have proven that we can still separate the peaks and reconstruct the energy of the incident protons with

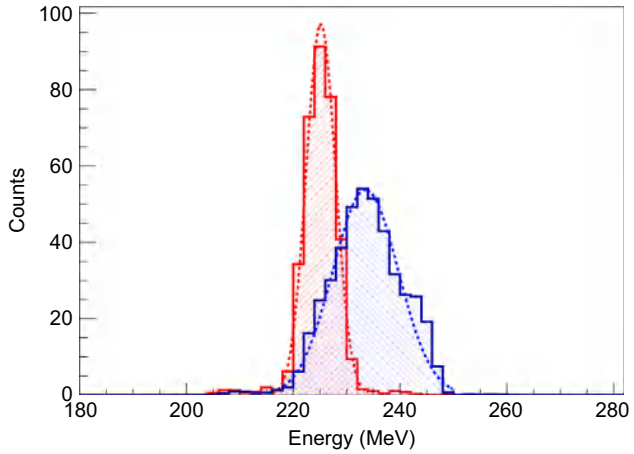

Fig. 9. Projection of the two-dimensional $\Delta E-E$ plots corresponding to two different runs at 225 and 235 MeV onto the calibration line C of Fig. 8.

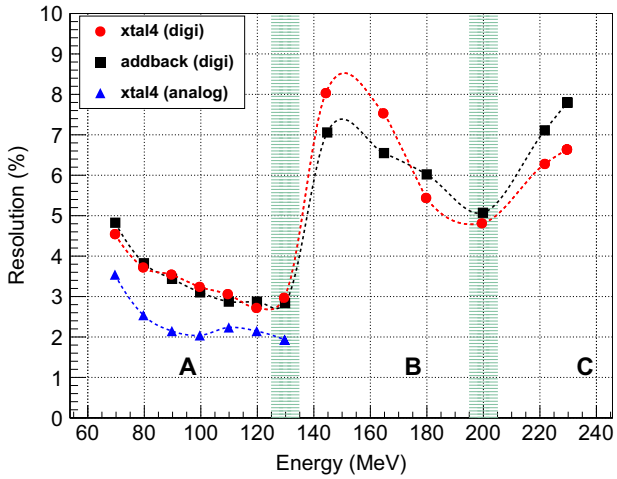

Fig. 10. Energy resolution as a function of the proton energy. The first vertical shaded region is at the energy in which the Bragg peak lies on the limit between the two crystals. The second vertical shaded region is at the energy in which the Bragg peak lies on the edge of the second crystal. Beyond this point the protons pass through the entire length of the phoswich unit.

a resolution of 7% at 230 MeV, and expect a resolution around 10–15% at 280–300 MeV. One could improve the energy resolution at these energies by increasing the length of the second crystal and therefore increasing the total punch-through energy.

3. Conclusions

A high-resolution scintillator array for the detection and spectroscopy of gamma rays and protons has been constructed: CEPA4. It is made of four individual phoswich modules based on the optical coupling of 4 cm of $LaBr_3$(Ce) to 6 cm of $LaCl_3$(Ce). The detector response to medium and high energy protons has been measured at the CCB cyclotron facility. For the first time we have demonstrated that we can reconstruct the incident energy of the protons even if they have sufficient energy to punch through the entire length of the crystal. In this context we have measured an energy resolution of 7% for 220 MeV protons. This detector, although conceived and built as a prototype towards the final design of CEPA for CALIFA at R^{3}B-FAIR, might find its own applications in experiments investigating β-decay as well as low-energy reactions with radioactive beams due to its high performance in gamma-ray and proton spectroscopy. Furthermore, the authors are exploring its applications to medical physics, in particular to perform high-accuracy dosimetry in hadron-therapy with ^{12}C beams as well as proton tomography.

Acknowledgments

This work was partly financed by the Spanish Research funding agency: Ministerio de Economía y Competitividad under project FPA2012-32443, and partly through FP7 by the Era-Net NuPNET/03/12 (GANAS) project. We thank the staff of the Bronowice Cyclotron Centre (CCB) for their kind help and for providing stable proton beams for our measurements.

References

[1] P. Kitching, et al., Advanced Physics Particles Nuclei 15 (1985) 43.
[2] P.G. Hansen, et al., Annual Review of Nuclear Particle Science 53 (2003) 219.
[3] T. Aumann, et al., Physical Review C 88 (2013) 064610.
[4] T. Aumann, B. Jonson, Technical Proposal for the Design, Construction, Commissioning and Operation of R3B, A Universal Setup for Kinematical

Complete Measurements of Reactions with Relativistic Radioactive Beams. URL ⟨http://www-win.gsi.de/r3b/Documents/R3B-TP-Dec05.pdf⟩.
[5] W. Henning, Nuclear Physics A 805 (2008) 502c.
[6] I. Augustin, Nuclear Instruments and Methods in Physics Research Section B 261 (2007) 1014, and references therein.
[7] D. Cortina, et al., Nuclear Data Sheets 120 (2014) 99.
[8] The CALIFA Collaboration, CALIFA Barrel Technical Design Report, 2012. URL ⟨http://www.fair-center.eu/for-users/experiments/nustar/nustar-documents/technical-design-reports.html⟩.
[9] O. Tengblad, et al., Nuclear Instruments and Methods in Physics Research Section A 704 (2013) 19.
[10] Saint-Gobain Crystals. URL ⟨http://www.crystals.saint-gobain.com/⟩.
[11] URL ⟨http://www.ifj.edu.pl/ccb/⟩.
[12] Hamamatsu Photonics. URL ⟨http://www.hamamatsu.com/⟩.
[13] CAEN Electronic Instrumentation. URL ⟨http://www.caen.it⟩.
[14] International Commission on Radiation Units and Measurements, ICRU Report 49, 1993.
[15] S. Agostinelli, et al., Nuclear Instruments and Methods in Physics Research Section A 506 (2003) 250.
[16] MESYTEC Detector Readout Systems. URL ⟨http://www.mesytec.com/⟩.